SUPPLEMENTARY MATERIALS

Identification of a robust methylation predictor for cutaneous melanoma diagnosis

Kathleen Conway[1,2,3], Sharon N. Edmiston[3], Joel S. Parker[3,4], Pei Fen Kuan[5], Yi-Hsuan Tsai[3], Pamela A. Groben[2,6], Daniel C. Zedek[2,6], Glynis A. Scott[7,8], Eloise A. Parrish[3], Honglin Hao[2], Michelle V. Pearlstein[2], Jill S. Frank[3], Craig C. Carson[2], Matthew D. Wilkerson[11], Xiaobei Zhao[3], Nathaniel A Slater[2], Stergios J. Moschos[3,10], David W. Ollila[3,9], Nancy E. Thomas[2,3]

Affiliations of authors:

[1]Department of Epidemiology, School of Public Health, University of North Carolina, Chapel Hill, NC; [2]Department of Dermatology, School of Medicine, University of North Carolina, Chapel Hill, NC; [3]Lineberger Comprehensive Cancer Center (LCCC), University of North Carolina at Chapel Hill, Chapel Hill, NC; [4]Department of Genetics, School of Medicine, University of North Carolina, Chapel Hill, NC; [5]Department of Applied Mathematics and Statistics, Stony Brook University, Stony Brook, NY; [6]Department of Pathology and Laboratory Medicine, School of Medicine, University of North Carolina, Chapel Hill, NC; [7]Department of Dermatology, University of Rochester School of Medicine, Rochester, NY; [8]Department of Pathology and Laboratory Medicine, University of Rochester School of Medicine, Rochester, NY; [9]Department of Surgery, School of Medicine, University of North Carolina, Chapel Hill, NC; [10]Department of Medicine, School of Medicine, University of North Carolina, Chapel Hill, NC; [11]Department of Anatomy, Physiology & Genetics, Uniformed Services University of the Health Sciences, Bethesda, MD

SUPPLEMENTARY METHODS

Dermatopathology histopathological interobserver review

Histopathological review of all samples was conducted independently by three expert dermatopathologists (PG, DZ, GS) to assign diagnoses of melanoma or nevus or to identify a melanocytic proliferation of uncertain malignant potential ('uncertain' sample). Five μm-thick tissue sections were cut from each tissue block containing melanoma, nevus, or uncertain sample and were mounted on uncoated glass slides. A hematoxylin and eosin (H&E)-stained slide of each tissue was initially reviewed by an expert dermatopathologist at UNC to assign diagnosis, classify histopathologic subtype, score standard histopathological features, and evaluate each sample for adequacy of formalin-fixation, tissue size, percent melanocytic cells, and percent necrosis. This reviewer also encircled the melanocytic tissue areas on the H&E slides for use as guides in manual microdissection. Two additional expert dermatopathologists reviewed the same set of melanocytic samples using H&E-stained slides or high-resolution Aperio images and assigned diagnoses of melanoma, nevus, or uncertain. In the final assignment of diagnosis, melanocytic samples were assigned diagnoses of melanoma or nevus only if there was complete consensus between the three dermatopathologists and the original pathology report. However, we did not exclude a lesion as melanoma if the majority of dermatopathologists interpreted the lesion as melanoma and visceral metastases and/or death from melanoma provided unequivocal evidence of the malignancy of the lesion. Melanocytic samples were considered uncertain if there was interobserver disagreement in the diagnosis of melanoma versus nevus between any of the three dermatopathologists or the original pathology report, or if any dermatopathogist or the pathology report described the sample as having an uncertain diagnosis. Based on the pathology report alone, 30 of the melanocytic lesions were uncertain; however, taking into account the subsequent dermatopathologist reviews, seven nevi (based on the pathology report) and four

melanomas (based on the pathology report) were reclassified as uncertain. Details of the histopathology for the melanocytic samples that were successfully profiled using the 450K arrays are provided in Table 1. The diagnostic interpretations (based on the original pathology report and the three dermatopathology reviewers) for the uncertain samples are in Supplementary Figure S8.

Illumina Infinium HumanMethylation450 Beadchip analysis

Sodium bisulfite modified DNA (120ng) was processed through the Illumina Infinium HD FFPE Restore protocol according to the manufacturer's instructions. Genome-wide DNA methylation profiling was performed on Restore-treated DNA from melanocytic samples using the Illumina Infinium HumanMethylation450 BeadChip (450K) array in the Mammalian Genotyping Core at UNC. Samples were analyzed in three batches that included mixtures of melanomas, nevi, melanocytic proliferations of uncertain malignant potential, positive (fully methylated) and negative (unmethylated) controls, and melanoma cell line controls (MCF7, VMM39, A375). BeadArrays were scanned and data assembled using the Illumina BeadStudio methylation module (v 3.2). Each CpG methylation data point is represented by fluorescent signals from the M (methylated; Cy5) and U (unmethylated; Cy3) alleles. Background intensity computed from a set of negative controls was subtracted from each data point. The methylation level of individual CpG sites was determined by calculating the β value, defined as the ratio of the fluorescent signal from the methylated allele to the sum of the fluorescent signals of both the methylated and unmethylated alleles. β values range from 0 (completely unmethylated) to 1.0 (fully methylated). Infinium HumanMethylation450 BeadChip data were imported into R (http://cran.r-project.org).

Methylation array data preprocessing and filtering

Preprocessing of the Infinium HumanMethylation450 BeadChip methylation dataset (n = 485,557 probes) was performed by removing probes (n = 41,937) mapping to more than one location in the genome (Price et al., 2013), with any missing values or poor-performing probes with detection *P*-values > 0.05 in over 20% of the samples, probes on the X and Y chromosomes, and additional probes overlapping a SNP (n = 56; Illumina tech note link). Beta mixture quantile (BMIQ) normalization (Teschendorff et al., 2013) was then applied to the methylation β values for correction of bias due to the type I and type II probe sets. Three melanomas, one nevus, and one uncertain sample (of the 203 samples) failed array analysis due to inadequate DNA quantity and/or quality. The final dataset contained 383,229 probes and 203 samples (89 melanomas, 73 nevi, 41 uncertain, plus 12 controls).

Statistical analyses

To develop a binary diagnostic classifier distinguishing melanomas from nevi, the sample set of melanomas and nevi with diagnostic consensus was randomly split into a training set (67% of each sample class) and an independent validation set (the remaining 33%). Uncertain samples lacking diagnostic consensus were excluded from model training and validation. Multiple predictive models based on different CpG probe sets, including models accounting for patient age, were tested for their ability to distinguish melanomas from nevi, as described below. For each probe set, Monte-Carlo cross validation with 100 iterations was performed on training samples using the ElasticNet algorithm implemented in R package glmnet (Zou and Hastie, 2005) to obtain optimal parameters (alpha and the number of probes) for automatic selection of a subset of probes that best differentiate melanomas. In each iteration, 2/3 of the training set was

randomly selected to build the elastic model and to predict on the rest of 1/3 in the training set. Based on the average AUC across 100 iterations, we determined the number of probes to be included in the final model. Finally, we calculated the classifier score using the β value of selected probes in the final model. Heatmaps depicting methylation levels at diagnostic probes in melanomas and nevi were generated in R using Euclidean distance and average linkage clustering. Columns were annotated with diagnostic category, sample set, and age. PCA was performed on the methylation matrix (centered to zero and scaled to unit variance one) to illustrate the segregation of melanomas and nevi.

Diagnostic models tested

Multiple models based on different probe sets or their combinations were tested for their ability to distinguish melanomas from nevi. First, to allow for future validation using the new Illumina Infinium MethylationEPIC (850K) array, we limited CpG probes in all models to those that were on both the 450K and EPIC (850K) arrays (maximum n = 358,049). Second, we further tested models that restricted probes to those associated with specific 'candidate genes' (according to Illumina annotation) that were previously found to be differentially methylated between melanomas and nevi in our prior study (Conway et al., 2011) using the Illumina Cancer Panel I methylation array (maximum n= 6,003). Within each of these probe sets, we imposed several additional levels of filtering. We assessed the effect of limiting probes to those exhibiting larger differential methylation between melanomas and nevi (with IQR > 0.2 β). Because melanoma patients are typically older than those biopsied for nevi (as in this study), we addressed the potential effect of age on probe selection by testing the inclusion of patient age in the model, the effect of removing probes significantly associated with age in linear regression analysis of logit

transformed β values (probes with $P < 0.01$; n = 271,892 or 4,324 probes associated with 'candidate' genes), or adjusting for age after exclusion of age-associated probes. Finally, we also tested only probes with annotation indicating genomic location in one or more genes. In total, we tested 19 models in the training set.

Analysis of association of methylation with patient age

A linear regression model on logit transformed β values was employed to determine whether individual CpG probes, including those selected as part of the diagnostic predictor defining differences between melanomas and nevi, were associated with patient age. The Benjamini-Hochberg false discovery rate (FDR) was used to control for multiple comparisons, and probes significantly associated with age were significant at $P < 0.01$.

Gene ontology analysis

The DAVID Bioinformatics Resources 6.7 Functional Annotation Tool (https://david.ncifcrf.gov/) was used to perform gene-GO term enrichment analysis to identify the most relevant GO terms associated with the 38 genes found to be diagnostic for melanomas versus nevi. Entrez gene IDs for each gene were compared to the human whole genome background. We performed functional annotation clustering with default settings.

Independent validation in published methylation datasets

Illumina 450K methylation data for TCGA-SKCM (skin cutaneous melanomas; 105 primary and 367 metastatic) were downloaded from the Broad Institute Firehose web portal (http://firebrowse.org/) (version 2016012800). β values for each of the 40 CpG probes were

converted to 0s if they were 'NA'. The final prediction model was applied using the β values to calculate a classifier score for each melanoma sample. A heatmap and waterfall plot, ordered left to right according to increasing classifier score, display β values and corresponding classifier scores for TCGA primary melanomas and the melanomas and nevi in the UNC/UR dataset. Boxplots illustrate the range of classifier scores for TCGA primary and metastatic melanomas versus UNC/UR samples. Illumina 450K methylation data for 33 primary melanomas, 28 metastatic melanomas, and 14 nevi were obtained from Gene Expression Omnibus (GEO) (accession number GSE86355) from the study of Wouters et al (2017). Diagnostic classifier scores, AUC, sensitivity, and specificity were determined as described for the UNC/UR samples. Illumina Infinium HumanMethylation27 (27K) methylation data for 24 melanomas and 5 nevi were also downloaded from GEO (accession number GSE45266) from the study of Gao et al (2013). Methylation β values at 44 probes corresponding to 38 diagnostic predictor genes were median centered and used to generate a heatmap in R using Spearman rank correlation and average linkage clustering.

mRNA expression associated with diagnostic genes in an independent dataset

The Affymetrix Hu133A gene expression dataset from Talantov et al (2005) with 18 nevi and 45 primary melanomas was downloaded from GEO (accession number GSE3189). Expression levels were summarized to the gene level by selecting the probe set with highest standard deviation for each gene. Expression data for each gene were median-centered and clustered in R using Spearman rank correlation and average linkage. Principal component analysis was also performed to illustrate the segregation between melanomas and nevi.

References

Conway K, Edmiston SN, Khondker ZS, Groben PA, Zhou X, Chu H, et al. DNA-methylation profiling distinguishes malignant melanomas from benign nevi. Pigment Cell Melanoma Res 2011;24(2):352-60.

Gao L, Smit MA, van den Oord JJ, Goeman JJ, Verdegaal EM, van der Burg SH, et al. Genome-wide promoter methylation analysis identifies epigenetic silencing of MAPK13 in primary cutaneous melanoma. Pigment Cell Melanoma Res 2013;26(4):542-54.

Price ME, Cotton AM, Lam LL, Farre P, Emberly E, Brown CJ, et al. (2013) Additional annotation enhances potential for biologically-relevant analysis of the Illumina Infinium HumanMethylation450 BeadChip array. Epigenetics Chromatin. 6:4.

Talantov D, Mazumder A, Yu JX, Briggs T, Jiang Y, Backus J, et al. Novel genes associated with malignant melanoma but not benign melanocytic lesions. Clin Cancer Res 2005;11(20):7234-42.

Teschendorff AE, Marabita F, Lechner M, Bartlett T, Tegner J, Gomez-Cabrero D, et al. (2013) A beta mixture quantile normalization method for correcting probe design bias in Illumina Infinium 450k DNA methylation data. Bioinformatics 29:189-196.

Thomas NE, Slater NA, Edmiston SN, Zhou X, Kuan PF, Groben PA, et al. DNA methylation profiles in primary cutaneous melanomas are associated with clinically significant pathologic features. Pigment Cell Melanoma Res 2014;27(6):1097-105.

Wouters J, Vizoso M, Martinez-Cardus A, Carmona FJ, Govaere O, Laguna T, et al. Comprehensive DNA methylation study identifies novel progression-related and prognostic markers for cutaneous melanoma. Bmc Med 2017;15(1):101.

Zou H, Hastie T. Regularization and variable selection via the Elastic Net. Journal of the Royal Statistical Society 2005; Series B (Statistical Methodology) (67):301-20.

Supplementary Table S1. Diagnostic accuracy of the 40 CpG classifier in patient subsets within the validation set

		Area Under the ROC Curve (AUC)	Sensitivity	Specificity	Positive Predictive Value	Negative Predictive Value
All patients		0.996	96.6%	100.0%	100.0%	96.2%
Patient or lesion characteristic						
Age	≤50	0.996	95.2%	100.0%	100.0%	98.4%
	>50	1.000	100.0%	100.0%	100.0%	100.0%
Sex	Male	0.999	98.2%	100.0%	100.0%	97.2%
	Female	1.000	100.0%	100.0%	100.0%	100.0%
Anatomic site of lesion	Trunk	1.000	100.0%	100.0%	100.0%	100.0%
	Head/neck/extremities	0.999	98.4%	100.0%	100.0%	97.3%
Lesion pigmentation	Heavy/Medium	0.999	98.6%	100.0%	100.0%	98.4%
	Absent	1.000	100.0%	100.0%	100.0%	100.0%
Solar elastosis in skin	Absent	1.000	100.0%	100.0%	100.0%	100.0%
	Mild to Severe	0.998	98.4%	100.0%	100.0%	90.0%
Tissue or technical factor						
Institutional tissue source	UNC-Chapel Hill	0.999	98.8%	100.0%	100.0%	98.5%
	Univ. of Rochester	1.000	100.0%	100.0%	100.0%	100.0%
Presence of lymphocytes	Moderate to brisk	0.998	98.7%	100.0%	100.0%	96.7%
	Absent or minimal	1.000	100.0%	100.0%	100.0%	100.0%
% melanocytic cells	≥50%	1.000	98.5%	100.0%	100.0%	98.3%
	<50%	1.000	100.0%	100.0%	100.0%	100.0%

Supplementary Table S2. Top 50 functional annotation terms from DAVID GO analysis of 38 genes in the 40-CpG melanoma classifier for melanoma

Category	Term	Count	%	P value	List Total	Pop Hits	Pop Total	Fold Enrichment	Benjamini
INTERPRO	IPR012287:Homeodomain-related	7	18.4	3.56E-06	31	238	16659	15.8	1.14E-04
INTERPRO	IPR001356:Homeobox	7	18.4	3.31E-06	31	235	16659	16.0	1.59E-04
UP_SEQ_FEATURE	DNA-binding region:Homeobox	7	18.4	1.14E-06	36	190	19113	19.6	1.88E-04
INTERPRO	IPR017970:Homeobox, conserved site	7	18.4	3.07E-06	31	232	16659	16.2	2.95E-04
SMART	SM00389:HOX	7	18.4	1.49E-05	23	235	9079	11.8	4.16E-04
SP_PIR_KEYWORDS	Homeobox	7	18.4	4.46E-06	36	242	19235	15.5	4.77E-04
GOTERM_MF_FAT	GO:0043565~sequence-specific DNA binding	9	23.7	1.16E-05	26	607	12983	7.4	6.10E-04
GOTERM_MF_FAT	GO:0003700~transcription factor activity	11	28.9	6.28E-06	26	975	12983	5.6	6.59E-04
SP_PIR_KEYWORDS	developmental protein	9	23.7	6.21E-05	36	779	19235	6.2	3.32E-03
GOTERM_MF_FAT	GO:0030528~transcription regulator activity	11	28.9	2.79E-04	26	1512	12983	3.6	9.72E-03
SP_PIR_KEYWORDS	dna-binding	11	28.9	1.38E-03	36	1868	19235	3.1	4.80E-02
GOTERM_MF_FAT	GO:0003677~DNA binding	11	28.9	8.10E-03	26	2331	12983	2.4	1.57E-01
GOTERM_MF_FAT	GO:0016563~transcription activator activity	5	13.2	7.33E-03	26	410	12983	6.1	1.76E-01
GOTERM_MF_FAT	GO:0001653~peptide receptor activity	3	7.9	2.01E-02	26	114	12983	13.1	2.99E-01
GOTERM_MF_FAT	GO:0008528~peptide receptor activity, G-protein coupled	3	7.9	2.01E-02	26	114	12983	13.1	2.99E-01
SP_PIR_KEYWORDS	Transcription	9	23.7	2.96E-02	36	2071	19235	2.3	4.15E-01
GOTERM_BP_FAT	GO:0048598~embryonic morphogenesis	5	13.2	3.95E-03	30	307	13528	7.3	4.28E-01
SP_PIR_KEYWORDS	transcription regulation	9	23.7	2.64E-02	36	2026	19235	2.4	4.35E-01
SP_PIR_KEYWORDS	disease mutation	8	21.1	2.25E-02	36	1591	19235	2.7	4.56E-01
GOTERM_BP_FAT	GO:0051252~regulation of RNA metabolic process	11	28.9	3.23E-03	30	1813	13528	2.7	4.97E-01
GOTERM_CC_FAT	GO:0044459~plasma membrane part	10	26.3	7.63E-03	23	2203	12782	2.5	5.28E-01
GOTERM_BP_FAT	GO:0030326~embryonic limb morphogenesis	3	7.9	1.48E-02	30	87	13528	15.5	5.47E-01
GOTERM_BP_FAT	GO:0035113~embryonic appendage morphogenesis	3	7.9	1.48E-02	30	87	13528	15.5	5.47E-01
GOTERM_BP_FAT	GO:0048736~appendage development	3	7.9	2.04E-02	30	103	13528	13.1	5.48E-01
GOTERM_BP_FAT	GO:0060173~limb development	3	7.9	2.04E-02	30	103	13528	13.1	5.48E-01
GOTERM_BP_FAT	GO:0002009~morphogenesis of an epithelium	3	7.9	1.97E-02	30	101	13528	13.4	5.69E-01
GOTERM_BP_FAT	GO:0060429~epithelium development	4	10.5	1.24E-02	30	227	13528	7.9	5.85E-01
GOTERM_MF_FAT	GO:0042277~peptide binding	3	7.9	5.77E-02	26	203	12983	7.4	5.90E-01
GOTERM_BP_FAT	GO:0045449~regulation of transcription	12	31.6	1.47E-02	30	2601	13528	2.1	5.93E-01
GOTERM_BP_FAT	GO:0035108~limb morphogenesis	3	7.9	1.89E-02	30	99	13528	13.7	5.94E-01
GOTERM_BP_FAT	GO:0035107~appendage morphogenesis	3	7.9	1.89E-02	30	99	13528	13.7	5.94E-01
GOTERM_BP_FAT	GO:0035295~tube development	4	10.5	1.14E-02	30	220	13528	8.2	6.20E-01
GOTERM_BP_FAT	GO:0001501~skeletal system development	4	10.5	3.02E-02	30	319	13528	5.7	6.32E-01
GOTERM_BP_FAT	GO:0035239~tube morphogenesis	3	7.9	3.01E-02	30	127	13528	10.7	6.60E-01
GOTERM_BP_FAT	GO:0050877~neurological system process	7	18.4	4.03E-02	30	1210	13528	2.6	6.63E-01
GOTERM_BP_FAT	GO:0045165~cell fate commitment	3	7.9	3.55E-02	30	139	13528	9.7	6.65E-01
GOTERM_BP_FAT	GO:0035136~forelimb morphogenesis	2	5.3	4.61E-02	30	22	13528	41.0	6.71E-01
GOTERM_CC_FAT	GO:0044456~synapse part	3	7.9	6.62E-02	23	246	12782	6.8	6.73E-01
GOTERM_BP_FAT	GO:0045944~positive regulation of transcription from RNA polymerase II promoter	4	10.5	4.42E-02	30	371	13528	4.9	6.76E-01
GOTERM_BP_FAT	GO:0006350~transcription	9	23.7	6.92E-02	30	2101	13528	1.9	6.76E-01
GOTERM_BP_FAT	GO:0010557~positive regulation of macromolecule biosynthetic process	5	13.2	4.93E-02	30	654	13528	3.4	6.76E-01
GOTERM_BP_FAT	GO:0007507~heart development	4	10.5	1.07E-02	30	215	13528	8.4	6.79E-01
GOTERM_BP_FAT	GO:0035115~embryonic forelimb morphogenesis	2	5.3	4.00E-02	30	19	13528	47.5	6.84E-01
GOTERM_BP_FAT	GO:0014032~neural crest cell development	2	5.3	6.84E-02	30	33	13528	27.3	6.85E-01
GOTERM_BP_FAT	GO:0014033~neural crest cell differentiation	2	5.3	6.84E-02	30	33	13528	27.3	6.85E-01
GOTERM_BP_FAT	GO:0006355~regulation of transcription, DNA-dependent	11	28.9	2.74E-03	30	1773	13528	2.8	6.87E-01
GOTERM_BP_FAT	GO:0009891~positive regulation of biosynthetic process	5	13.2	5.92E-02	30	695	13528	3.2	6.91E-01
GOTERM_BP_FAT	GO:0031328~positive regulation of cellular biosynthetic process	5	13.2	5.67E-02	30	685	13528	3.3	6.92E-01
GOTERM_BP_FAT	GO:0006357~regulation of transcription from RNA polymerase II promoter	5	13.2	6.76E-02	30	727	13528	3.1	6.95E-01
GOTERM_BP_FAT	GO:0046620~regulation of organ growth	2	5.3	6.24E-02	30	30	13528	30.1	6.95E-01

Supplementary Figure S1. Comparative performance of 40-CpG melanoma classifier models tested in primary melanomas and nevi in the training set. The training set (67% of samples, randomly selected) consisted of 60 melanomas and 48 nevi with diagnostic consensus between all 3 dermatopathologists and the initial pathology report. AUC versus number of probes are shown for each diagnostic model tested. The broken line in all plots indicates AUC of 0.98. Eight diagnostic models were tested in panels a and b that contained as starting probe sets either (a) all available 450K probes (overlapping probes on the EPIC 850K methylation array) or (b) 450K probes associated with candidate genes differentially methylated between melanomas and nevi in our prior Illumina Cancer Panel I methylation study (Conway et al., 2011; Thomas et al., 2014). The eight models tested within each of the two probe sets were as follows: (1) all 450K or 'candidate gene' probes (----), (2) probes filtered for IQR > 0.2 β (····), (3) model adjusted for age (age-adjusted) (----), (4) model adjusted for age (age-adjusted), and probes filtered for IQR > 0.2 β (····), (5) age-associated probes removed from model (age-independent) (----), (6) age-associated probes removed from model (age-independent), and probes filtered for IQR > 0.2 β (····), (7) age-associated probes removed, and model adjusted for age (age-independent, age-adjusted) (----), (8) age-associated probes removed, and model adjusted for age (age-independent, age-adjusted), and probes filtered for IQR > 0.2 β (····). Models that did not account for age (models 1 or 2) provided the highest diagnostic accuracy with fewest probes. (c) Comparison of models derived from all 450K/IQR > 0.2 β versus candidate/IQR > 0.2 β. (d) Comparison of models derived from all 450K/IQR > 0.2 β versus 450K/IQR > 0.2 β and restricted to probes with Illumina gene annotation.

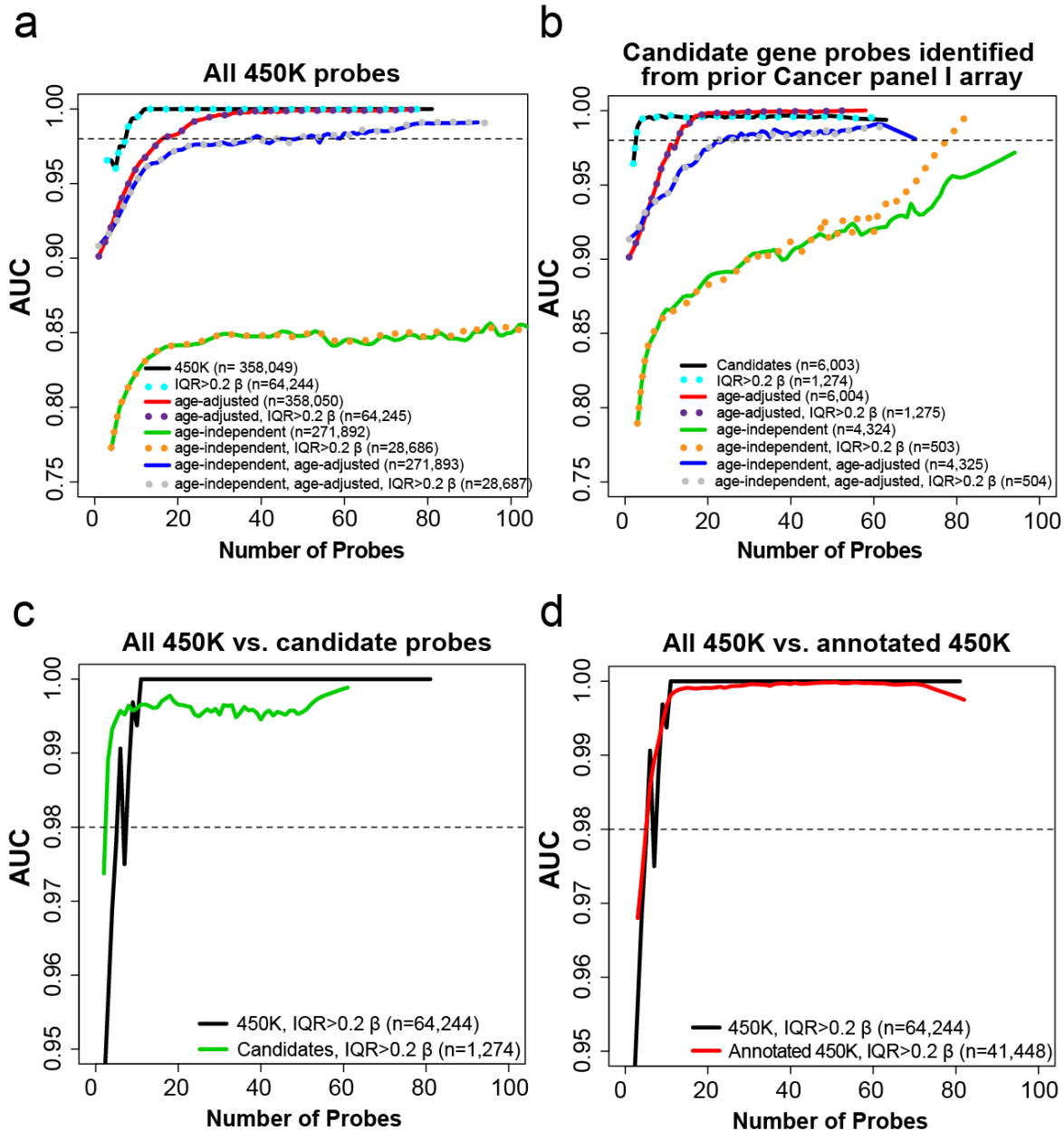
a
All 450K probes
AUC
Number of Probes
450K (n= 358,049)
IQR>0.2 β (n=64,244)
age-adjusted (n=358,050)
age-adjusted, IQR>0.2 β (n=64,245)
age-independent (n=271,892)
age-independent, IQR>0.2 β (n=28,686)
age-independent, age-adjusted (n=271,893)
age-independent, age-adjusted, IQR>0.2 β (n=28,687)
b
Candidate gene probes identified from prior Cancer panel I array
AUC
Number of Probes
Candidates (n=6,003)
IQR>0.2 β (n=1,274)
age-adjusted (n=6,004)
age-adjusted, IQR>0.2 β (n=1,275)
age-independent (n=4,324)
age-independent, IQR>0.2 β (n=503)
age-independent, age-adjusted (n=4,325)
age-independent, age-adjusted, IQR>0.2 β (n=504)
c
All 450K vs. candidate probes
AUC
Number of Probes
450K, IQR>0.2 β (n=64,244)
Candidates, IQR>0.2 β (n=1,274)
d
All 450K vs. annotated 450K
AUC
Number of Probes
450K, IQR>0.2 β (n=64,244)
Annotated 450K, IQR>0.2 β (n=41,448)

Supplementary Figure S2. Boxplots illustrating differential methylation at the 40 classifier and neighboring CpGs in melanomas and nevi. Boxplots show methylation at classifier CpGs (red) and, if present, nearby CpGs (black) within 500 base pairs upstream or downstream of the classifier CpGs. *P* values were determined by the Wilcoxon test. (a) Classifier CpGs hypermethylated in melanomas compared with nevi. (b) Classifier CpGs hypomethylated in melanomas compared with nevi.

Figure S2.

a **Hypermethylated in melanomas compared with nevi**

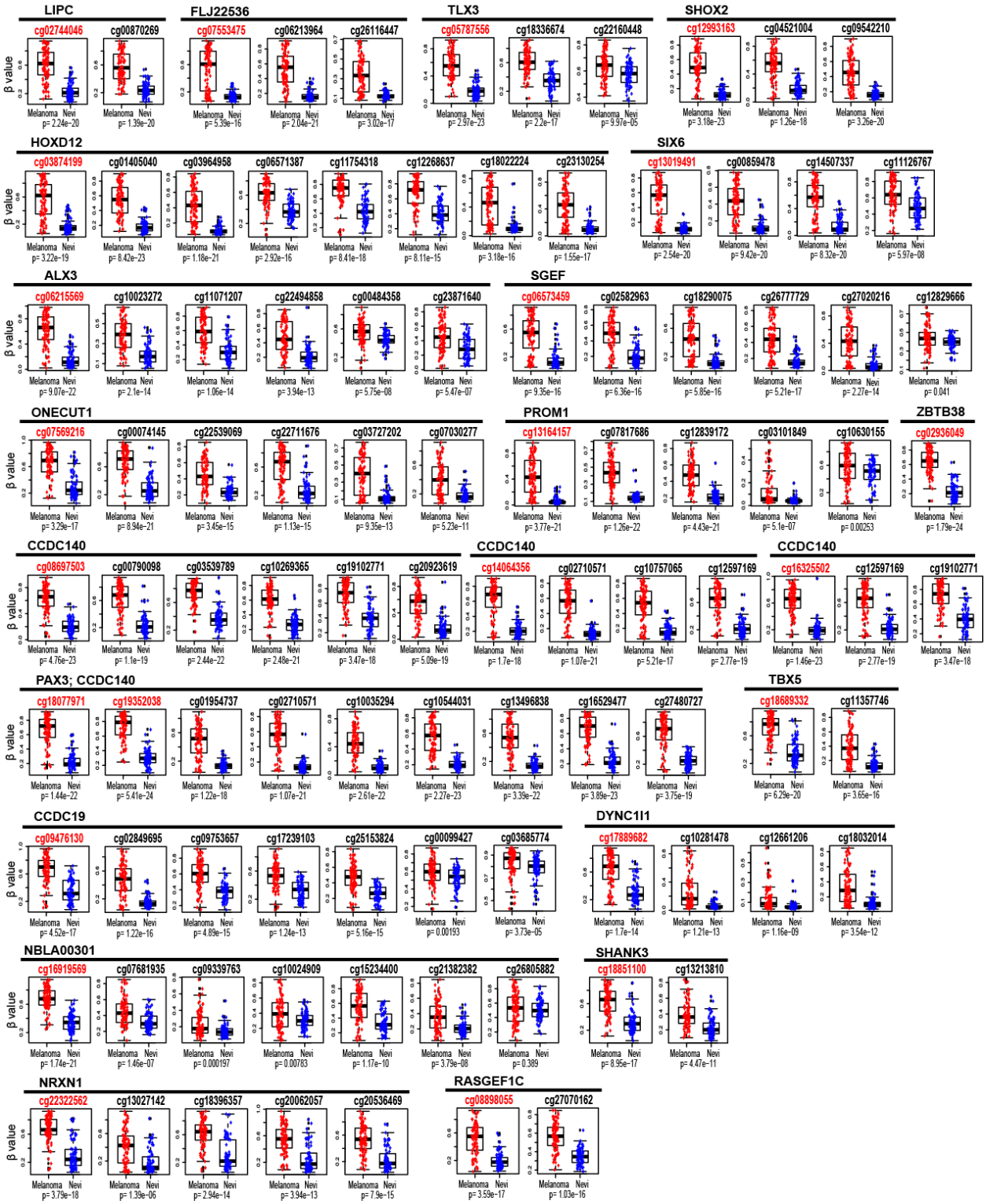

Figure S2

b Hypomethylated in melanomas compared with nevi

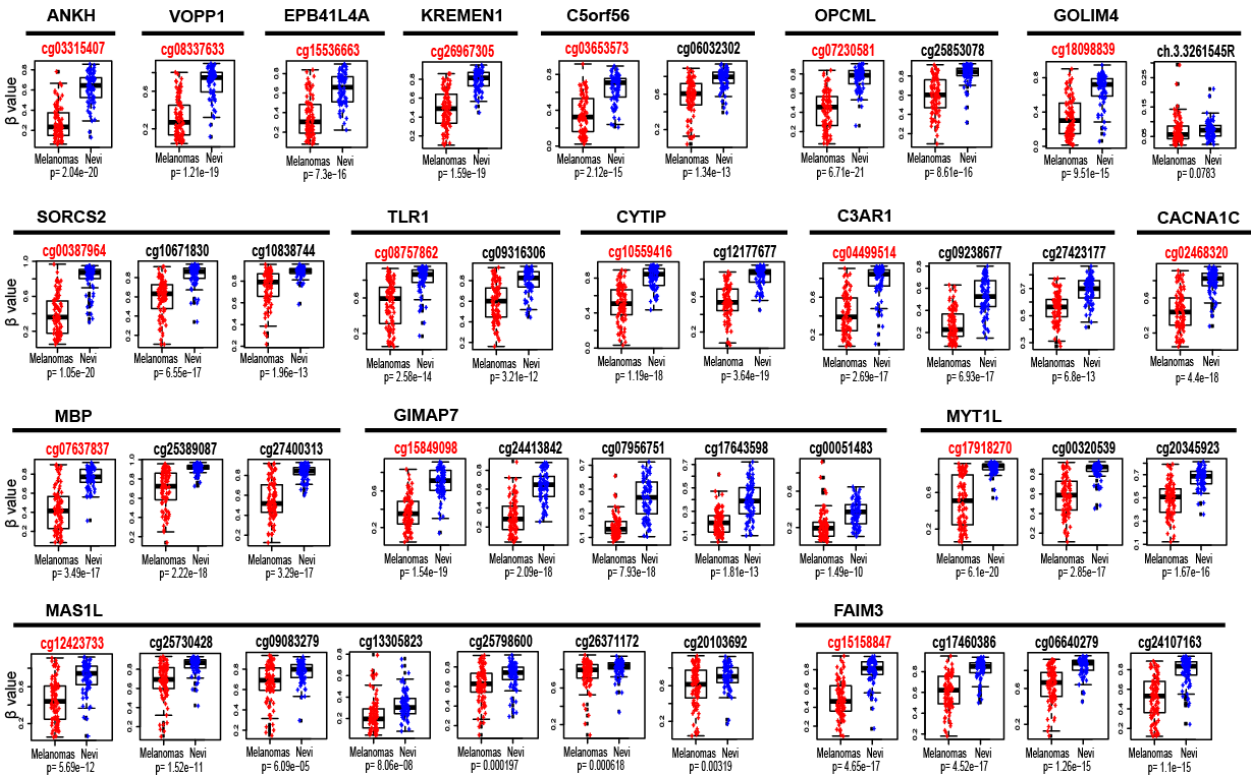

Supplementary Figure S3. Heatmaps showing methylation at the 40 classifier CpGs in the primary melanomas and nevi in the UNC/UR training and validation sets. The clinical and pathologic characteristics of the samples are annotated.

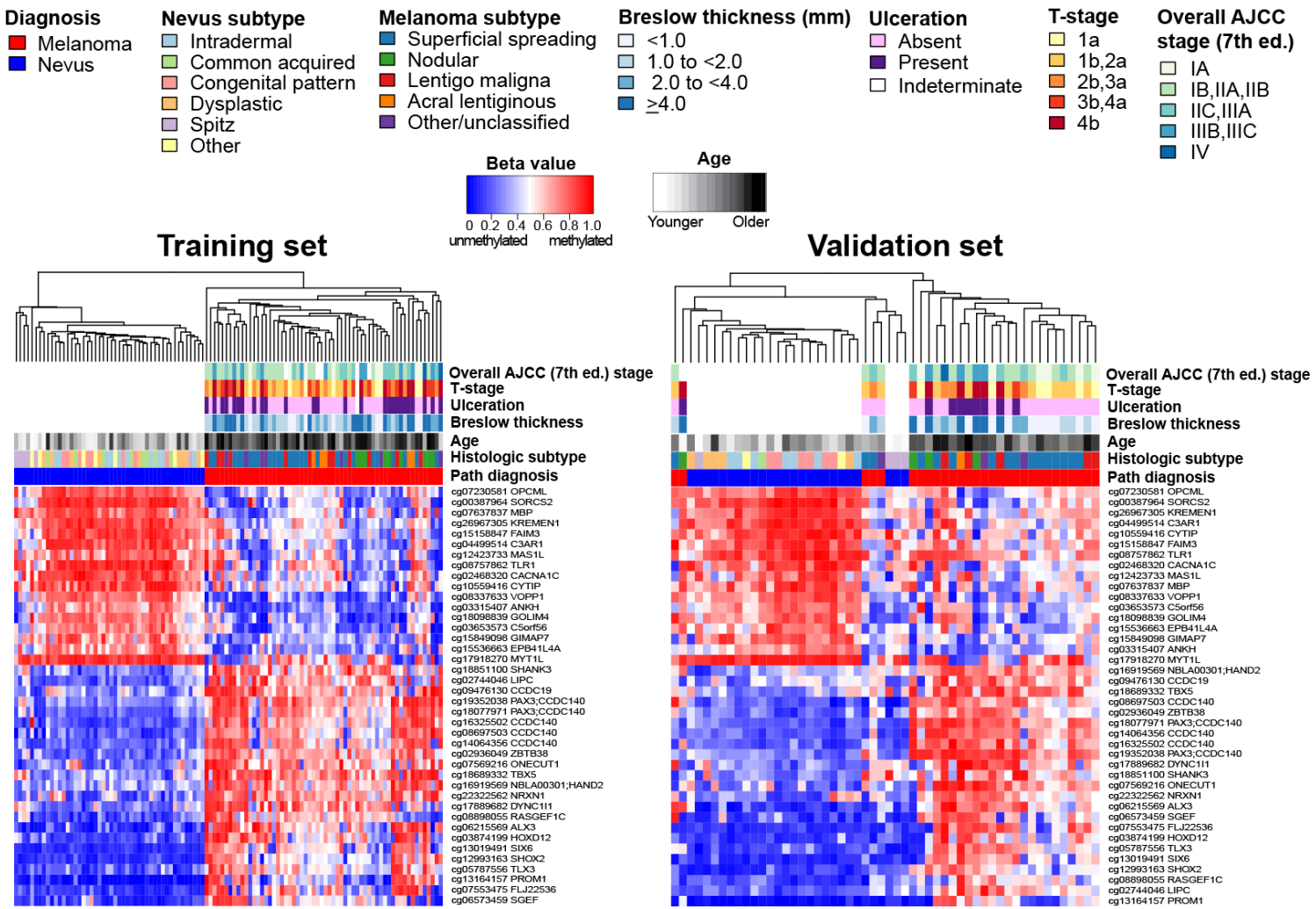

Supplementary Figure S4. Boxplots of classifier scores according to clinical staging features in the primary melanomas in the UNC/UR training and validation sets. The median and interquartile range are encompassed by each box. The broken line indicates the classifier score threshold for distinguishing melanomas from nevi.

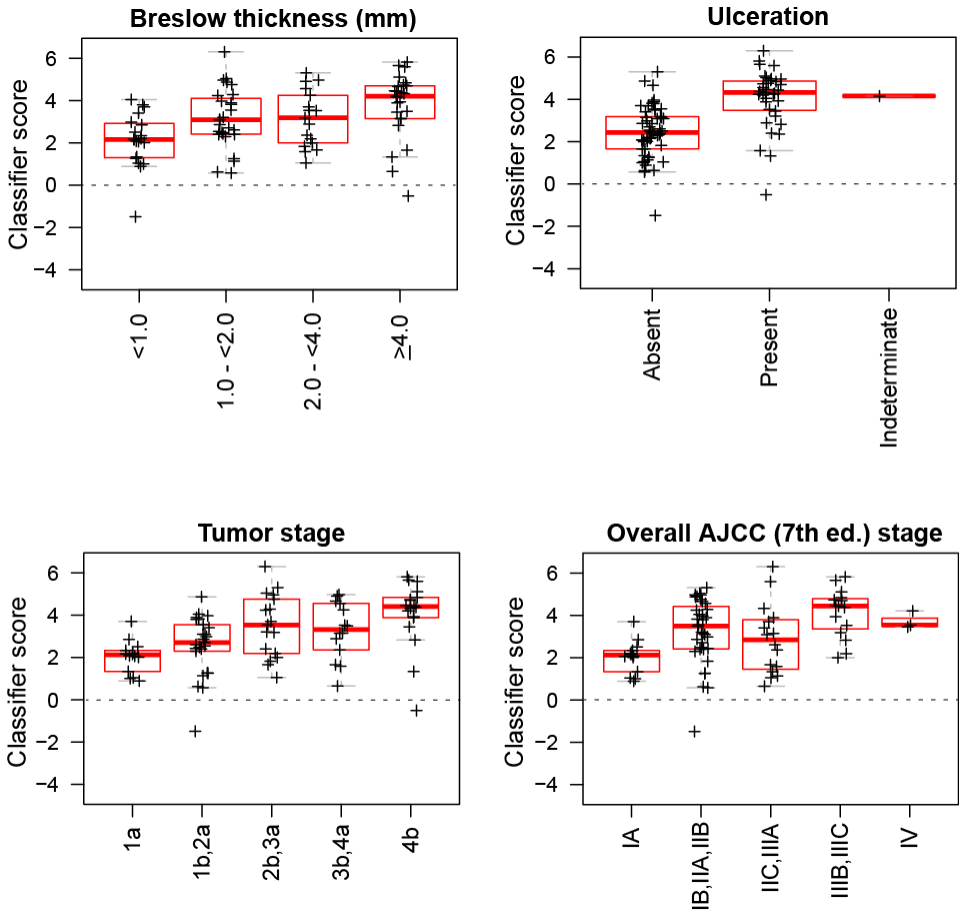

Supplementary Figure S5. Performance of the 40-CpG melanoma classifier according to patient age. (a) AUC, sensitivity, specificity, PPV, and NPV for all histopathology-confirmed melanoma and nevus patients younger (≤ 50 years of age) (left plot) or older (> 50 years of age) (right plot) at diagnosis. (b) Scatter plot of 40-CpG diagnostic classifier score (y axis) versus patient age for all melanoma, nevus, and diagnostically uncertain samples (x axis).

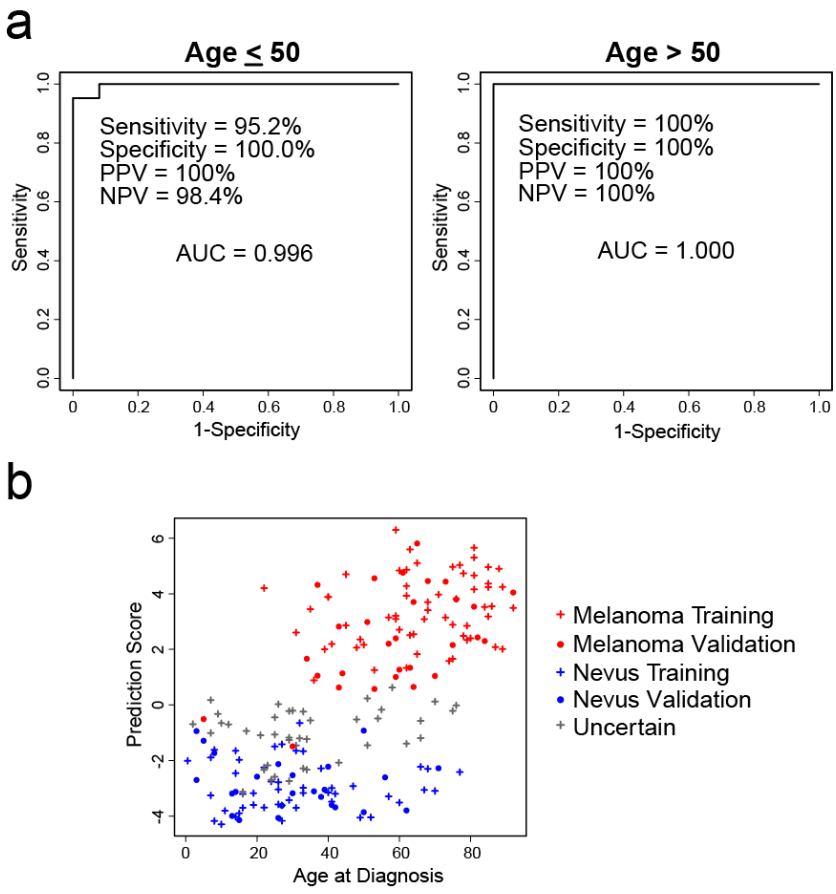

Supplementary Figure S6. Independent validation of differential mRNA expression at genes diagnostic for melanoma. The Affymetrix Hu133A gene expression dataset from Talantov *et al* (2005) was obtained from GEO (accession number GSE3189). (a) Heatmap illustrating mRNA expression for 25 (of 38) diagnostic genes in 45 primary melanomas and 18 nevi. (b) mRNA expression-based PCA plot showing separation of melanomas from nevi.

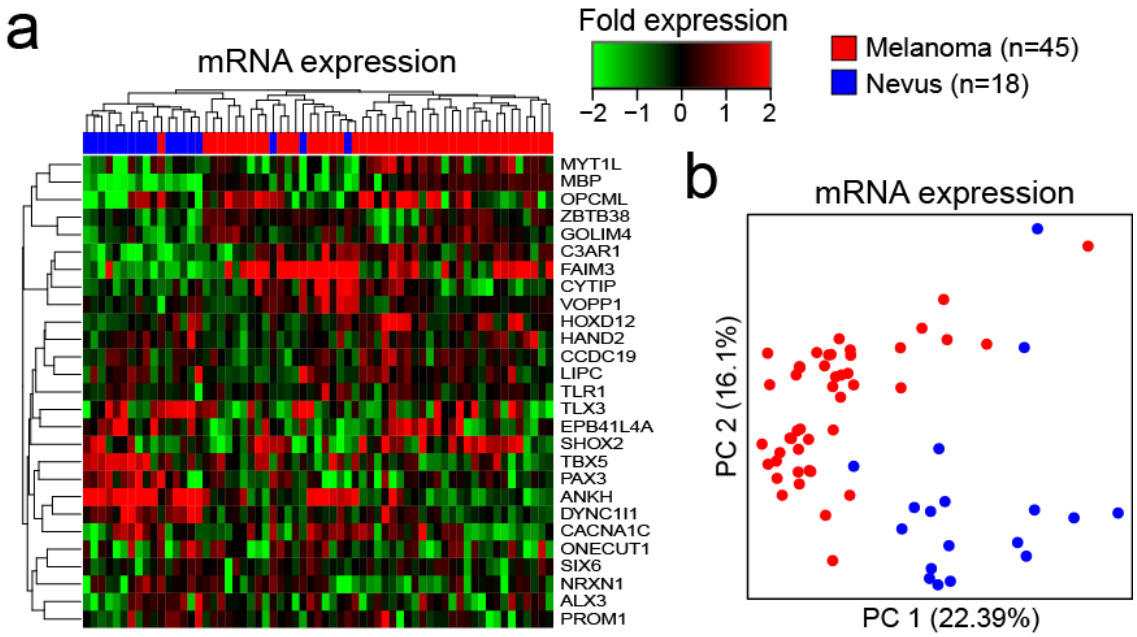

Supplementary Figure S7. PCA plots showing separation of melanomas, nevi and diagnostically uncertain samples by different probe sets. Uncertain melanocytic samples fell among pathologically-confirmed nevi or between melanomas and nevi in PCA plots when using: (a) 40 classifier probes, or (b) 41,448 probes obtained after filtering for IQR > 0.2 β and Illumina gene annotation.

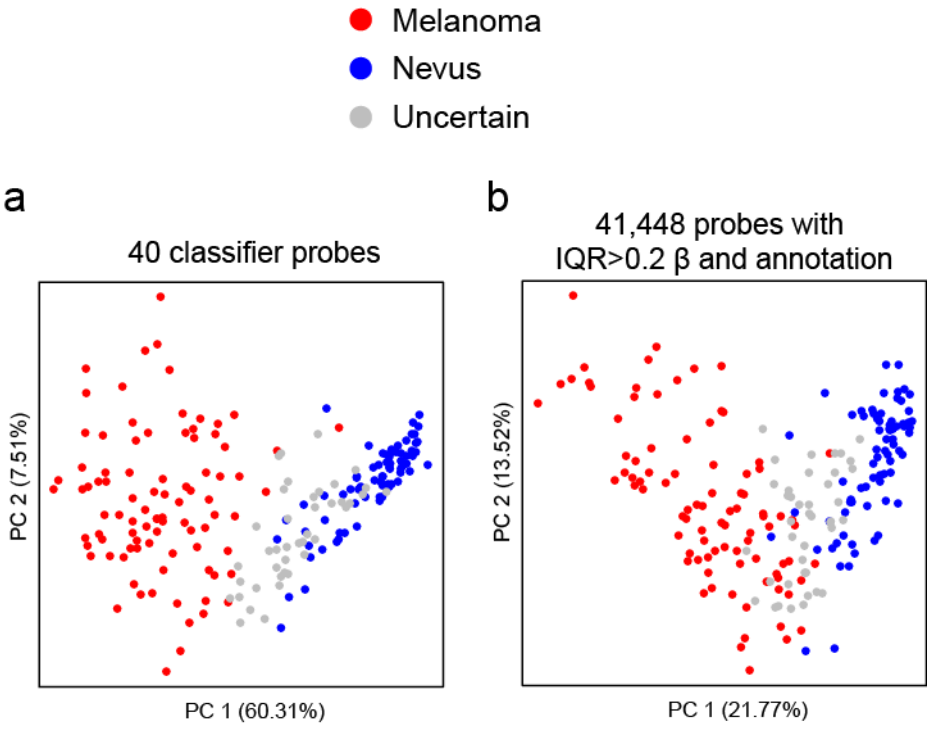

Supplementary Figure S8. Diagnostic calls by pathologists versus the 40-CpG classifier for the 41 uncertain melanocytic samples. Diagnostic calls by pathologists were nevus (blue), melanoma (red) or uncertain (gray) (top panel). The original pathology classification was based on the initial pathology report. Interobserver review was subsequently conducted by three expert dermatopathologists. The 41 uncertain samples lacked consensus among these four levels of pathology review. 40-CpG classifier scores and diagnostic calls for the 41 uncertain samples are shown, ordered from lowest to highest (lower panel).